Myxoid Epithelioid Gastrointestinal Stromal Tumor (GIST) With Mast Cell Infiltrations: A Subtype of GIST With Mutations of Platelet-Derived Growth Factor Receptor Alpha Gene

SHINJI SAKURAI, MD, TADASHI HASEGAWA, YUJI SAKUMA, YUTAKA TAKAZAWA, ATSUSHI MOTEGI, TAKASHI NAKAJIMA, KEN SAITO, MASASHI FUKAYAMA, AND TADAKAZU SHIMODA

We analyzed 30 gastrointestinal stromal tumors (GISTs) that were immunohistochemically weak or negative for KIT. Histologically, all 30 GISTs consisted of epithelioid tumor cells in at least a part of the tumor. The tumor cells showed different morphologies and arranged themselves in different histological patterns. In 20 of the 30 GISTs, round or oval epithelioid tumor cells often showed a less cohesive pattern of growth and showed eosinophilic cytoplasm and peripherally placed nuclei with myxoid stroma, whereas in the remaining 10 cases, tumor cells were arranged in a more cohesive pattern without myxoid stroma. The former type of tumors is called *myxoid epithelioid GISTs* in this study. Subsequent mutational analyses showed that the platelet-derived growth factor receptor alpha (*PDGFRA*) gene mutations in exon 12 or exon 18 were identified in 20 (66.7%) of the 30 GISTs, and especially in 18 (90%) of the 20 myxoid epithelioid GISTs. Moreover, 17 (85%) of the 20 myxoid epithelioid GISTs were accompanied by mast cell infiltrations within the tumor nodules. In the remaining cases, 2 (6.7%) of the 30 GISTs had c-*kit* gene mutations in exon 11, and no mutation was found in 8 (26.7%) of 30 GISTs. None of the patients with myxoid epithelioid GISTs died of disease. These results suggest that myxoid epithelioid GISTs are a distinct subtype of GISTs that are closely correlated with the *PDGFRA* gene mutation and that recognition of such histological characteristics should be helpful for molecular subclassification of GISTs that are important for molecular targeting therapy by imatinib mesylate (STI571). HUM PATHOL 35:1223-1230. © 2004 Elsevier Inc. All rights reserved.

Key words: GISTs, myxoid epithelioid, mast cell infiltration, *PDGFRA* gene mutation.

Abbreviations: GISTs, gastrointestinal stromal tumors; PDGFRA, platelet-derived growth factor receptor alpha; ICCs, interstitial cells of Cajal; PCR, polymerase chain reaction.

Gastrointestinal stromal tumors (GISTs) are the most frequent nonepithelial neoplasm in the stomach and intestine.[1-5] In the past, most GISTs were thought to originate from smooth muscle, based on their histological features. However, recent reports clarified the close relationship between GISTs and interstitial cells of Cajal (ICCs), which play important roles, such as as the pacemaker that enables cooperative peristalsis or as the mediator of nitric oxide–mediated transmission from nerve terminals to smooth muscle cells in the gastrointestinal tract.[6,7] Simultaneous expression of specific molecules such as KIT, CD34, the embryonic isoform of myosin heavy chain (SMemb), and nestin in both ICCs and GISTs[8-12] leads us to consider that GISTs may develop from ICCs or their progenitor cells. In previous reports, about 90% of GISTs were immunohistochemically positive for KIT,[8-12] and mutations of the c-*kit* gene have been found in most of these KIT-positive GISTs.[13] Recently, mutations of the platelet-derived growth factor receptor alpha (*PDGFRA*) gene encoding platelet-derived growth factorα have been reported in GISTs that are negative for c-*kit* gene mutations.[14,15]

Histopathologically, most GISTs consist of spindle tumor cells with acidophilic fibrillary cytoplasm and elongated or cigar-shaped nuclei with perinuclear vacuoles. In our experience, these typical GISTs are usually KIT positive by immunohistochemical staining. On the other hand, tumor cells show pleomorphic or epithelioid histology in rare cases of GISTs, and such histology is sometimes difficult for pathologists to diagnose. In such cases, an immunohistochemically positive result for KIT is a useful marker for the diagnosis of GISTs.

However, in our previous analyses, we found that KIT immunoreactivity in epithelioid cells of GISTs was weaker than in spindle cells in the same tissue sections or other tumors. Moreover, some GISTs were completely negative for KIT. Lack of the c-*kit* gene mutation had also been reported in GISTs with an epithelioid component.[16] In such cases, accuracy of the diagnosis of GISTs may be questionable. In this study, to clarify the clinicopathologic features and molecular genetic background of such tumors, we analyzed 27 cases of

From the Department of Pathology, Jichi Medical School, Tochigi, Department of Pathology, National Cancer Center Research Institute and Hospital, Tokyo, Department of Pathology, Graduate School of Medicine, University of Tokyo, Tokyo, and Department of Tumor Pathology, Gunma University Graduate School of Medicine, Maebashi, Gunma, Japan. Accepted for publication July 1, 2004.

Supported by a Grant-in-Aid for Scientific Research from the Ministry of Education, Science, Sports, and Culture of Japan and by a Grant-in-Aid for Cancer Research from the Ministry of Health, Labor and Welfare of Japan.

Address correspondence and reprint requests to Shinji Sakurai, MD, 3311-1 Yakushiji, Minamikawachi-machi, Kawachi-gun, Tochigi 329-0498, Japan.

0046-8177/$—see front matter

doi:10.1016/j.humpath.2004.07.008

TABLE 1. Risk Category for Gastrointestinal Stromal Tumor Based on the MIB-1 Grading System and Tumor Size

	Tumor size (cm)		
Grade*	≤5	<5-≤10	>10
Low	Low risk	Intermediate risk	High risk
High	High risk	High risk	High risk

*Low grade, MIB-1–labeling index of <10% and no tumor necrosis; high grade, MIB-1–labeling index of ≥10% or tumor necrosis.

GISTs showing weak or negative staining for KIT. From the results of histological findings and mutational analyses of the c-*kit* and the *PDGFRA* gene, we showed that specific histology of GISTs was closely correlated with the *PDGFRA* gene mutation and termed such GISTs *myxoid epithelioid GISTs*.

MATERIALS AND METHODS

KIT-Weak or KIT-Negative GISTs

The study was approved by the research ethics committee of Jichi Medical School. Of the 303 GISTs collected at Jichi Medical School Hospital, National Cancer Center Hospital, and related hospitals, all of which were analyzed by the immunohistochemical techniques described in this section, 30 (9.9%) primary GISTs showing negative or weak immunostaining for KIT were selected. A consensus judgment was adopted as the proper immunohistochemical score of the tumor on the basis of strength: 0, negative; 1+, weak staining; 2+, moderate staining; 3+, strong staining. Tissue mast cells, which stain 2+ or 3+, were used as internal positive controls for KIT. The distribution of positive cells was also recorded in an effort to impart the diffuse or focal nature of the positive cells: sporadic (positive cells <10%), focal (10% to <50% positive cells), or diffuse (50% positive cells). The immunohistochemical scores of 0 and 1+ with focal to diffuse distribution were considered to be KIT-weak or KIT-negative GISTs.

Of these, 29 GISTs were surgically resected from 29 patients, and the remaining 1 was from an autopsy case in which the patient died of hypoxic encephalopathy (case 22). The sites of the primary tumors were the stomach (n = 26), esophagus (n = 1), small intestine (n = 1), and omentum (n = 2). One patient (case 17) was treated with imatinib mesylate because of the residual tumor in the omentum. Formalin-fixed and paraffin-embedded specimens were used for histopathologic and immunohistochemical studies and for mutational analyses for the c-*kit* and *PDGFRA* genes. All GISTs were graded as high, intermediate, or low risk according to tumor size and to the MIB-1 grading system described elsewhere,[17] based on tumor differentiation, existence of tumor necrosis, and proliferating activity as estimated by Ki-67 (MIB-1) immunohistochemistry. Briefly, high-risk GISTs are >10 cm or are high grade (MIB-1–labeling index = 10% or tumor necrosis), intermediate-risk GISTs are >5 cm to 10 cm and are low grade (MIB-1–labeling index of <10% and no tumor necrosis), and low-risk GISTs are 5 cm and are low grade (Table 1).

Immunohistochemical Study

Immunohistochemical evaluation was performed by the avidin-biotin-peroxidase complex method in 3-μm-thick sections of formalin-fixed and paraffin-embedded specimens of GISTs and other mesenchymal tumors. We used polyclonal antibodies for KIT (DakoCytomation, Glostrup, Denmark: working dilution, 1:50; IBL, Fujioka, Japan: working dilution, 1:100), and a monoclonal antibody for CD34 (Becton Dickinson, Mountain View, CA: working dilution, 1:20). Cellular differentiation in GISTs was characterized by using the following antibodies: α-smooth muscle actin (DakoCytomation; monoclonal; working dilution, 1:500) and desmin (DakoCytomation; monoclonal; working dilution, 1:100) as markers for smooth muscle cells and by using the S100 protein (DakoCytomation; polyclonal, 1:1000) as a marker for Schwann cells. Ki-67 (MIB-1; MBL, Nagaoya, Japan: monoclonal, 1:100) was used to assess the proportion of proliferating cells, and the MIB-1–labeling index was estimated as reported elsewhere.[17] For antigen retrieval, formalin-fixed sections were pretreated in a microwave oven before incubation with the primary antibody.

We also performed toluidine blue staining for detection of mast cell infiltrations in GISTs. In the same KIT-stained sections of GISTs, we found many mast cell infiltrations between tumor cells. To accurately evaluate mast cell infiltrations in the tumors, toluidine blue staining was performed on all 3-μm-thick sections of formalin-fixed and paraffin-embedded specimens of GISTs in this study. For comparison, 24 cases of KIT-positive typical GISTs, all of which had c-*kit* gene mutations (23 in exon 11 mutations and 1 in exon 9) as shown by reverse-transcription polymerase chain reaction (PCR) and direct sequencing (data not shown), were also analyzed.

Sequencing Analyses of the C-*Kit* and *PDGFRA* Genes

Previously identified mutational hot spots in the c-*kit* and the *PDGFRA* gene in GISTs were analyzed. Genomic DNA was extracted from the 30 formalin-fixed and paraffin-embedded tumor tissues, by a standard proteinase K digestion method. Then the genomic DNA was amplified by PCR with the primers listed in Table 2 to amplify exons 9, 11, 13, and 17 of the c-*kit* gene and exons 12 and 18 of the *PDGFRA* gene. Each of the amplified fragments was purified from a polyacrylamide gel, and direct sequencing was performed with a Thermo Sequenase II Dye Terminator Cycle Sequencing Premix Kit (Amersham Biosciences, Piscataway, NJ) and with an ABI

TABLE 2. Sequences of Primers Used In This Study

Exon	Sequence
	c-kit
Exon 9F	5'-ATGCTCTGCTTCTGTACTGCC-3'
Exon 9R	5'-CAGAGCCTAAACATCCCCTTA-3'
Exon 11F	5'-CCAGAGTGCTCTAATGACTG-3'
Exon 11R	5'-ACCCAAAAAGGTGACATGCA-3'
Exon 13F	5'-CATCAGTTTGCCAGTTGTGC-3'
Exon 13R	5'-ACACGGCTTTACCTCCAAATG-3'
Exon 17F	5'-TGTATTCACAGAGACTTGGC-3'
Exon 17R	5'-GGATTTACATTATGAAAGTCACAGG-3'
	PDGFRA
Exon 12F	5'-TCCAGTCACTGTGCTGCTTC-3'
Exon 12R	5'-GCAAGGGAAAAGGGAGTCTT-3'
Exon 18F	5'-ACCATGGATCAGCCAGTCTT-3'
Exon 18R	5'-AAGTGTGGCAGGATCAGCCTG-3'

Abbreviation: PDGFRA, platelet-derived growth factor-α.

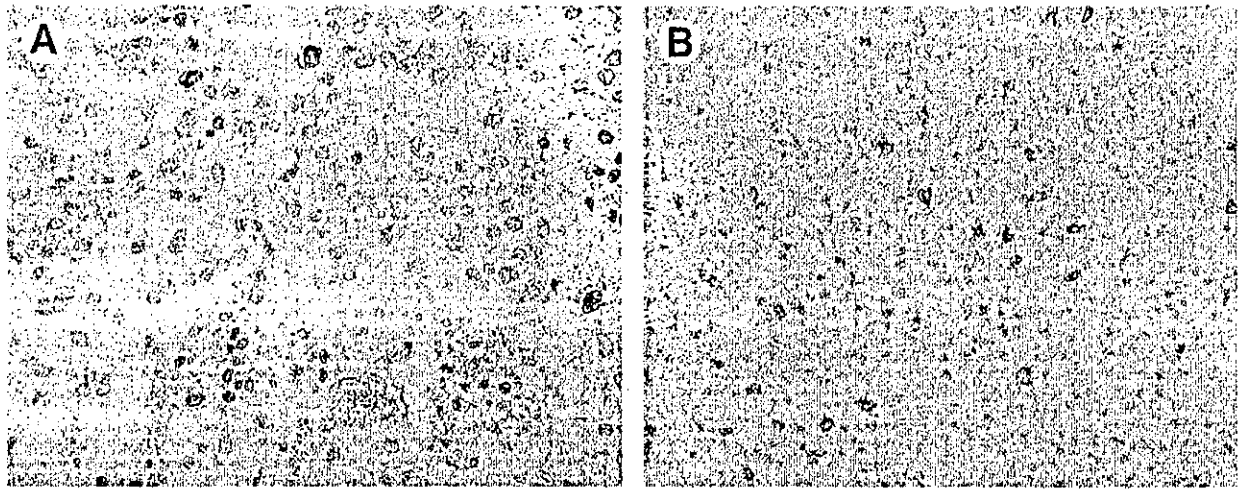

FIGURE 1. Immunostaining for KIT. All 27 gastrointestinal stromal tumors in this study were weak (A) or negative (B) for KIT. Strong immunoreactivity to KIT was observed in infiltrating mast cells in both cases.

PRISM 377 DNA Sequencer (Applied Biosystems, Foster City, CA), using the same primers as were used for PCR. All sequencing reactions were performed in both the forward and reverse directions.

Statistical Analyses

For the statistical analyses, we compared GISTs with and without myxoid epithelioid patterns (described in the results) and compared GISTs with or without the *PDGFRA* gene mutations. Gender, primary site, tumor grade, histological types, immunohistochemical phenotypes, and the existence of mast cell infiltrations were evaluated by Fisher's exact test or by χ^2 test. Age at surgery, maximum size of the tumors, and the MIB-1–labeling indexes were compared by Mann-Whitney U test.

RESULTS

Of the 30 GISTs examined in this study, 26 showed weak positive immunostaining for KIT according to our criteri, and the remaining cases (cases 20, 22, 25, and 26) were completely negative for KIT (Fig 1A and B). The clinicopathologic data resulting from the immunohistochemistry and mutational analyses of the c-*kit* and *PDGFRA* genes are presented in Table 3. The MIB-1–labeling index ranged from 1% to 21%. According to the criteria described above, 10 of the 30 tumors were classified as low risk, 6 as intermediate risk, and the remaining as high risk.

Histologically, all 30 GISTs showed epithelioid tumor cells in at least part of the tumor. Of these, we noticed that the tumor cells showed different morphology and arranged themselves in different patterns in each case with or without myxoid stroma. In cases 1, 2, 7, 11, 14, 19, 29, and 30, tumors consisted of both spindle and epithelioid tumor cells in varying ratios, and in the remaining cases, epithelioid cells occupied most parts of the tumor. In cases 1, 2, 3, 5, 7, 14, 17, 19, 27, and 29, the epithelial components of the tumor cells were mostly cohesive and arranged themselves in a sheetlike structure. Tumor cells in these cases showed clear or eosinophilic cytoplasm and centrally or peripherally placed nuclei (Fig. 2A).

On the other hand, in the remaining 17 cases of GISTs in this study, round or oval epithelioid tumor cells often showed a less cohesive pattern of growth and showed eosinophilic cytoplasm and peripherally placed nuclei with myxoid stroma. Multinucleated tumor cells were also seen in these tumors (Fig 2B), for which we used the term *myxoid epithelioid GISTs* in this study. Cases 6, 11, and 15, in which the myxoid epithelioid pattern was seen only in a part of the tumor, were also placed in this category.

Immunohistochemical Phenotypes

Of the 30 GISTs in the present study, 25 tumors were positive for CD34, and 13 tumors were weakly or focally positive for α-smooth muscle actin. Only 1 case was weakly positive for S100 protein, and 2 cases were weakly positive for desmin.

Mutations of the C-*kit* and *PDGFRA* Genes

Of the 30 GISTs examined here, 2 GISTs had c-*kit* gene mutations in exon 11 that were point mutations or in-frame deletions. *PDGFRA* gene mutations were found in 20 GISTs: 2 tumors had the same missense point mutation at codon 561 in exon 12, and the remaining tumors had in-frame deletions from codon 842 to 845 or had missense point mutations at codon 842 in exon 18. These are the same mutations of the *PDGFRA* gene in GISTs without the c-*kit* gene mutation, as previously reported. In the remaining 8 GISTs, mutations were not found in any exons of c-*kit* or *PDGFRA*.

TABLE 3. Clinicopathological Data Resulting From Immunohistochemistry and Mutational Analysis of the C-Kit and PDGFRA Gene in 27 Cases of KIT-Weak or KIT-negative GISTs

Case No.	Gender	Age	Primary Site	MIB-1 Size	MIB-1 LI (%)	MIB-1 Risk	Histology	Immunohistochemistry KIT	CD34	S100	SMA	Desmin	Mutations Gene	Mutations Site	Mast Cell Infiltration	Follow-Up Results (mo)
1	M	46	Small intestine	2.5	21	High	Spindle-cohesive epithelioid	Weak	+	+	−	−	—		—	DOD (22)
2	M	57	Esophagus	4.4	18	High	Spindle-cohesive epithelioid	Weak	+	−	−	−	c-kit	Exon 11 K558S, del V559	—	AW (16)
3	M	68	Stomach	7.5	<1	Int	Cohesive epithelioid	Weak	−	−	−	−	—		—	DOD (62)
4	M	60	Stomach	3.5	<1	Low	Myxoid epithelioid	Weak	+	−	−	−	PDGFRA	Exon 18 del DIMH842-845	+*	DOUD (364)
5	M	73	Stomach	3	8	Low	Cohesive epithelioid	Weak	−	−	+	−	—		—	AW (356)
6	M	46	Stomach	3	5	Low	Cohesive-myxoid epithelioid	Weak	+	−	−	−	—		—	AW (202)
7	F	71	Stomach	3.5	3	Low	Spindle-cohesive epithelioid	Weak	+	−	−	−	—		—	AW (190)
8	F	76	Stomach	2	9	Low	Myxoid epithelioid	Weak	+	−	+	−	PDGFRA	Exon 18 D842V	++†	AW (143)
9	M	43	Stomach	2.5	5	Low	Myxoid epithelioid	Weak	+	−	−	−	PDGFRA	Exon 18 D842V	—	AW (118)
10	M	44	Stomach	10	5	Int	Myxoid epithelioid	Weak	+	−	−	−	PDGFRA	Exon 18 del DIMH842-845	++	AW (101)
11	M	60	Stomach	12.5	3	High	Spindle-myxoid epithelioid	Weak	+	−	+	−	PDGFRA	Exon 18 del DIMH842-845, D846E	+	AW (96)
12	M	65	Stomach	3	3	Low	Myxoid epithelioid	Weak	+	−	−	−	—		+	AW (75)
13	M	50	Stomach	21	10	High	Myxoid epithelioid	Weak	+	−	+	+	PDGFRA	Exon 18 del DIMH842-845	+	AW (43)
14	M	62	Stomach	2.5	15	High	Spindle-cohesive epithelioid	Weak	+	−	−	+	c-kit	Exon 11 del MYEV552-555	—	AW (6)
15	M	46	Stomach	1.2	11	High	Cohesive-myxoid epithelioid	Weak	+	−	+	−	PDGFRA	Exon 18 D842V	—	AW (6)
16	F	73	Omentum	4	3	Low	Myxoid epithelioid	Weak	+	−	+	−	PDGFRA	Exon 18 D842V	++	AW (4)
17	M	52	Omentum	>20	4	High	Cohesive epithelioid	Weak	−	−	−	−	PDGFRA	Exon 18 del DIMH842-845	+	AW (13)
18	F	80	Stomach	3.7	3	Low	Myxoid epithelioid	Weak	+	−	−	−	PDGFRA	Exon 12 V561D	++	AW (3)
19	M	51	Stomach	2.5	2	Low	Spindle-cohesive epithelioid	Weak	+	−	+	−	—		—	DOUD (171)
20	M	65	Stomach	8	1	Int	Myxoid epithelioid	—	−	−	−	−	PDGFRA	Exon 12 V561D	++	ND
21	M	49	Stomach	8	14	High	Myxoid epithelioid	Weak	+	−	+	−	PDGFRA	Exon 18 del DIMH842-845	+	AW (12)
22	M	66	Stomach	1.2	49	Low	Myxoid epithelioid	—	−	−	−	−	PDGFRA	Exon 18 D842V	+	ND
23	M	54	Stomach	1.1	3	Low	Myxoid epithelioid	Weak	+	−	−	−	PDGFRA	Exon 18 D842V	++	AW (12)
24	M	74	Stomach	6	4.5	Int	Myxoid epithelioid	Weak	+	−	+	−	PDGFRA	Exon 18 D842V	+	AW (24)
25	F	36	Stomach	2.2	7.5	Low	Myxoid epithelioid	—	+	−	−	−	PDGFRA	Exon 18 del DIMH842-845	+	AW (9)
26	M	57	Stomach	6	5	Int	Myxoid epithelioid	—	+	−	+	−	PDGFRA	Exon 18 del DIMH842-845	+	AW (5)
27	F	64	Stomach	4	<1	Low	Cohesive epithelioid	Weak	+	−	−	−	—	—	AW (40)	
28	M	69	Stomach	6.5	2	Int	Myxoid epithelioid	Weak	+	−	+	−	PDGFRA	Exon 18 D842V	++	AW (1)
29	M	50	Stomach	4	5	Low	Spindle-cohesive epithelioid	Weak	+	−	+	−	PDGFRA	Exon 18 D842V	—	AW (3)
30	M	76	Stomach	2.3	9	Low	Spindle-myxoid epithelioid	Weak	+	−	+	−	PDGFRA	Exon 18 D842V	++	AW (1)

Abbreviations: PDGFRA, platelet-derived growth factor-α; GIST, gastrointestinal stromal tumor; LI, labeling index; SMA, smooth muscle actin; DOD, died of disease; del, deletion; AW, alive and well; int, intermediate; DOUD, died of unrelated disease; ND, no data available.

*For most cell infiltration instances.

†Numerous most cell infiltration instances present within a tumor nodule.

GISTs With or Without Mast Cell Infiltration

Mast cells were clearly detected by their characteristic metachromatic staining with toluidine blue. Infiltration of mast cells within the tumor nodules was observed in 18 of the 30 GISTs (60%; Fig 3A), although the number of infiltrating mast cells was varied in each case (Table 3). In contrast, no mast cell infiltration of 24 KIT-positive GISTs with c-*kit* gene mutations was observed (Fig 3B).

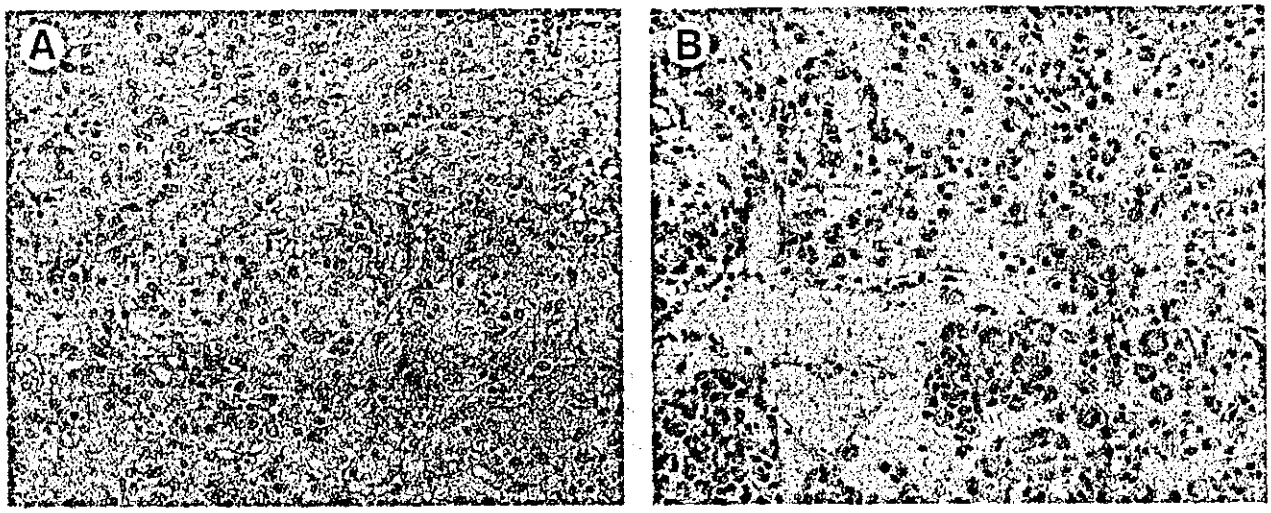

FIGURE 2. Epithelioid components of gastrointestinal stromal tumors in this study showed different histology. (A) Tumor cells in this case showed clear cytoplasm and centrally or peripherally placed nuclei and were mostly cohesive and arranged themselves in a sheetlike structure. (B) Tumor cells in other cases showed less cohesive patterns of growth and showed eosinophilic cytoplasm and peripherally placed nuclei with myxoid stroma. Multinucleated tumor cells were also seen in these tumors. Hematoxylin and eosin staining.

KIT-Weak or KIT-Negative GISTs With or Without Myxoid Epithelioid Patterns

The clinicopathologic data including other immunohistochemical data, the existence of mast cell infiltrations in the tumor nodules, and mutations of the c-*kit* or *PDGFRA* gene were compared between the 27 GISTs with or without myxoid epithelioid patterns (Table 4). The gender, age at initial operation, primary sites and sizes of tumors, MIB-1–labeling index and tumor risk, and immunohistochemical phenotypes were not different between the 2 groups. Mast cell infiltrations within the tumor nodules were preferentially observed in the GISTs with a myxoid epithelioid pattern ($P < 0.0001$). Only 1 weakly KIT-positive large GIST (case 19) without a myxoid epithelioid pattern was accompanied by mast cell infiltration. The presence or site of mutations in the *c-kit* or *PDGFRA* genes was significantly different between GISTs with and without a myxoid epithelioid pattern ($P < 0.0001$). Mutations in the *PDGFRA* gene were preferentially found in the GISTs with a myxoid epithelioid pattern (18 of 20, 90%), whereas only 2 of the 10 GISTs without a myxoid epithelioid pattern had a *PDGFRA* gene mutation (case 17). Two cases in GISTs without a myxoid epithelioid pattern (cases 2, 14) had a point mutation or an in-frame deletion in exon 11 of the c-*kit* gene.

Prognosis of the patients with KIT-weak or KIT-negative GISTs was as follows. Twenty-eight patients were followed for 1 to 364 months (mean, 82 months; median, 42 months). Four of the 28 patients died dur-

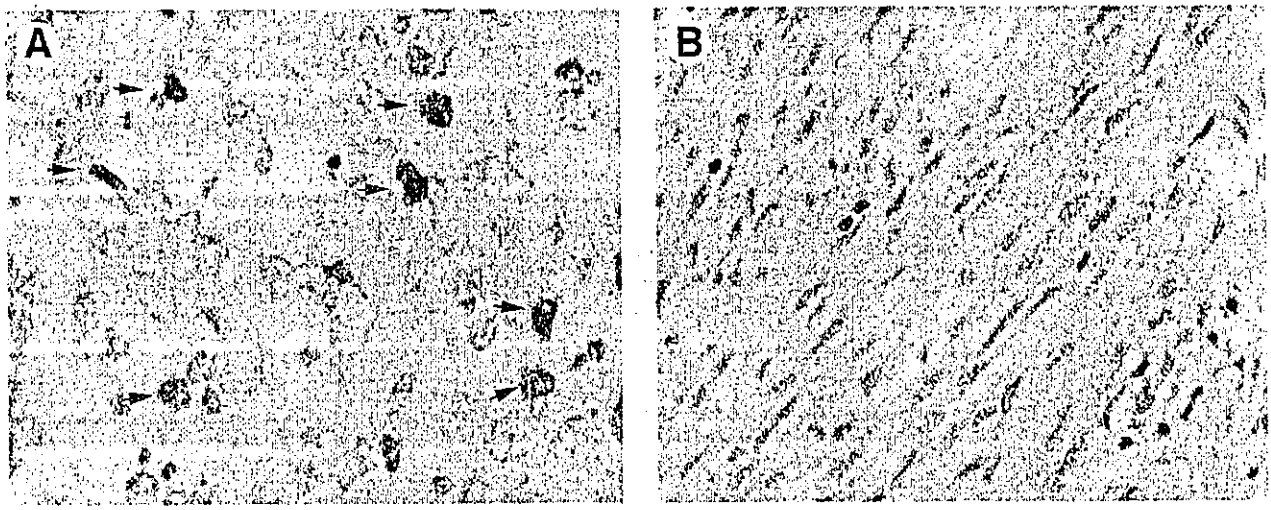

FIGURE 3. Mast cell infiltrations were frequently observed in KIT-weak or KIT-negative gastrointestinal stromal tumors (GISTs; arrow; A) but not in KIT-positive GISTs with *c-kit* gene mutations (B). Toluidine blue staining.

TABLE 4. Comparison of Clinicopathological and Immunohistochemical Data and Mutational Analysis of the C-Kit and PDGFRA Gene Between Myxoid Epithelioid GISTs and Others

Variable	KIT-Weak or KIT-Negative GISTs		*P* Value
	Myxoid Epithelioid GISTs (n = 20)	Others (n = 10)	
Gender (male:female)	16:4	9:1	NS
Age (yr)	36-80 (average, 59.5)	46-73 (average, 59.4)	NS
Site (eso/st/SI/ome)	0/20/0/1	1/7/1/1	NS
Size	5.4 ± 4.8	5.4 ± 5.3	NS
MIB-1 LI	5.4 ± 3.5	7.8 ± 7.5	NS
Grade (high/int/low)	4/5/11	4/1/5	NS
Immunohistory			
CD34	18/20	7/10	NS
SMA	10/20	3/10	NS
S100	0/20	1/10	NS
Desmin	1/20	1/10	NS
Mast cell infiltration	17/20	1/10	0.0001
Mutation (c-kit/PDGFRA/negative)	0/18/2	2/2/6	0.0001

Abbreviations: PDGFRA, platelet-derived growth factor-α; GIST, gastrointestinal stromal tumor; NS, statically not significant; eso, esophagus; St, stomach; SI, small intestine; LI, labeling index; SMA, smooth muscle actin.

ing the follow-up period, of which 2 deaths were caused by the primary disease (cases 1 and 3, each 22 and 62 months after initial operations) and the remaining deaths were caused by unrelated disease (cases 4 and 19). GISTs in cases 1 and 3 had no myxoid epithelioid component in the tumor cells or mutations in the c-*kit* and *PDGFRA* genes. None of the patients with myxoid epithelioid GISTs or GISTs with *PDGFRA* gene mutations died of disease during follow-up periods, although 1 patient had a residual tumor at the primary site (case 17).

DISCUSSION

In recent years, the diagnosis and treatment of GISTs has advanced and changed dramatically. Most GISTs consist of spindle cells showing fascicular patterns and are immunohistochemically positive for KIT.[8-12] Moreover, gain-of-function mutations in the c-*kit* gene are found in these KIT-positive GISTs.[8,13] Now, GISTs are defined as KIT-positive mesenchymal tumors in the gastrointestinal tract and are distinguished from other mesenchymal tumors. Recently, molecular targeting treatments with imatinib mesylate (STI571), which is a KIT tyrosine kinase inhibitor, have been given to patients with KIT-positive GISTs, with reports of significant effectiveness for metastatic and unresectable GISTs.[18,19]

However, it is known that some GISTs are immunohistochemically weak or negative for KIT. In such cases, the accurate diagnosis of GISTs might be difficult for pathologists, although the pathologic diagnosis is indispensable for correctly prescribing imatinib mesylate.

More recently, *PDGFRA* gene mutations have been reported in some GISTs without c-*kit* gene mutations that also can be effectively treated with imatinib mesylate.[14,15,20] However, the clinicopathologic and histological characteristics of GISTs with *PDGFRA* gene mutations have not been fully analyzed previously.

Overall, 30 of 303 GISTs (9.9%) were weak or negative for KIT and were analyzed in this study. All 30 GISTs consisted of epithelioid tumor cells exclusively or focally, although epithelioid GISTs are seen in about 20%-30% of all GISTs in general.[4,5,21] Of 273 KIT-positive GISTs in our cases, 226 (83%) GISTs were shown to be the spindle cell type, 38 (14%) were shown to be the mixed (combination of spindle and epithelioid cell) type, and 9 (3%) were shown to be the epithelioid cell type (data not shown). Histologically, we noticed different patterns within the epithelioid tumor cells in KIT-weak or KIT-negative GISTs. In some epithelioid GISTs, tumor cells arranged themselves in tightly cohesive patterns. In others, tumor cells loosely arranged themselves and were accompanied by myxoid stroma. We called the latter type of GISTs *myxoid epithelioid GISTs* in our study. Interestingly, subsequent mutational analyses showed a close relationship between these histological patterns and the type of mutations. Myxoid epithelioid GISTs closely correlated with *PDGFRA* gene mutations in both exons 12 and 18.

The *PDGFRA* gene mutations were found in 20 of the 30 KIT-weak or KIT-negative GISTs (66.6%). This rate is higher than that reported by Heinrich et al,[14] in whose study *PDGFRA* gene mutations were found in about 35% of GISTs without c-*kit* gene mutations. The rate became much higher when the cases were limited to the 20 myxoid epithelioid GISTs, of which 18 (90%) had *PDGFRA* gene mutations.

On the other hand, of 273 KIT-positive GISTs, 11 tumors were also accompanied by myxoid stroma, and 3 of those were of the epithelioid cell type resembling histology of myxoid epithelioid GISTs in this study. However, those 3 cases had mutations in the c-*kit* gene exon 11 but not in the *PDGFRA* gene (data not shown). Thus, the histology of myxoid epithelioid pattern in

KIT-weak or KIT-negative GISTs is considerably specific to GISTs with *PDGFRA* gene mutations. In only 2 GISTs with *PDGFRA* gene mutations (cases 17 and 29) were the GISTs not myxoid epithelioid. The tumor in case 17 was large and classified as high risk. Tumor progression may have influenced the morphology and growth pattern of the tumor cells in this case, although the tumor in case 29 was relatively small and was classified as low risk. In cases 6 and 12, *PDGFRA* gene mutations were not identified despite having a myxoid epithelioid pattern. However, the c-*kit* gene mutations were also not present in these cases. Mutations in other exons of the *PDFFRA* gene that we did not examine in this study might be present in these 2 tumors. Furthermore, we also found close relationships between myxoid epithelioid GISTs or GISTs with *PDGFRA* gene mutations and mast cell infiltration. In general, we frequently found mast cell infiltrations in various degrees in leiomyomas and leiomyosarcomas in the gastrointestinal tract and uterus.[22,23] Previous reports indicated that the numbers of mast cells within and around tumor nodules were thought to be a useful prognostic factor for soft tissue sarcomas.[23-25] In contrast, infiltrations of mast cells were observed in none of the KIT-positive GISTs with c-*kit* gene mutations in this study. We have used this histological difference for distinguishing between GISTs and other soft tissue tumors for some time. However, mast cell infiltration was observed in 18 of 30 GISTs (60%) in this study. Of these, 17 tumors were myxoid epithelioid GISTs (17 of 20, 85%). There is a close correlation between mast cell infiltrations and myxoid epithelioid patterns or *PDGFRA* gene mutations in GISTs ($P < 0.0001$). Very recently, Debiec-Rychter et al[26] also reported *PDGFRA* gene mutations in 3 (43%) of 7 KIT-negative GISTs, whereas their remaining tumors had no mutation in either c-*kit* or *PDGFRA* genes. In their reports, mast cell infiltrations were also seen within tumor nodule. Incidentally, mast cell infiltrations were not observed in 2 of 3 KIT-positive tumors resembling myxoid epithelioid GISTs in this study (data not shown).

At present, we have no evidence that explains the presence or absence of mast cell infiltrations among different types of GISTs. Stem cell factor (SCF), a natural ligand of the KIT receptor, is thought to be produced by smooth muscle cells and neurons in the gastrointestinal tract.[27,28] Mast cell infiltrations within leiomyomas and leiomyosarcomas are probably caused by SCF production by tumor cells that are of smooth muscle cell origin. On the other hand, SCF expression by tumor cells of GISTs has not been reported until now. However, we confirmed mRNA expression of both membrane-bound and soluble isoforms of SCF in all the KIT-positive GISTs by reverse-transcription PCR (data not shown). Rapid internalization of SCF by the SCF–KIT juxtacrine loop between tightly cohesive tumor cells may prevent mast cell infiltration in KIT-positive GISTs but not in myxoid epithelioid GISTs, which are less cohesive and weak or negative for KIT. Further studies about SCF expression in KIT-positive and KIT-weak or KIT-negative GISTs will be needed to explain the mechanism of mast cell infiltration in myxoid epithelioid GISTs.

GISTs are thought to originate from the ICCs because of the phenotypic similarity of specific molecules such as KIT, CD34, Smemb, and nestin.[8-12] However, in the human small intestine, a slow wave is also detected at the deep muscular plexus level, where KIT-positive ICCs are not present.[29] We previously observed KIT-negative, CD34-positive, ICC-like cells adjacent to KIT-positive ICCs in the stomach and small intestine.[11] The existence of KIT-negative fibroblast-like cells adjacent to KIT-positive ICCs has been reported.[30,31] GISTs with *PDGFRA* gene mutations may originate from such KIT-negative ICCs or other unknown mesenchymal cells, and that may reflect differences of histology and KIT expression. Further search and classification of ICCs and related mesenchymal cells and analysis of *PDGFRA* expression in such mesenchymal cells will be needed to confirm this hypothesis.

Although none of the patients with GISTs containing *PDGFRA* mutations died of disease, follow-up periods in this study are too short to conclude benign behavior of GISTs with *PDGFRA* mutations. Five of the 20 GISTs with the *PDGFRA* gene mutations were classified as high risk, and 1 of those (case 17) was treated with imatinib mesylate because of the residual tumor in the omentum. At present, the patient remains in partial remission. In this case, the mutation was deletion DIMH842-845 in exon 18 of the *PDGFRA* gene, and GISTs with this type of mutation have been reported to be sensitive to treatment with imatinib mesylate.[20] Mutational analysis and molecular subclassification of GISTs are now more important since the introduction of imatinib mesylate, because clinical responses to the drug and prognosis of patients are different in GISTs with different mutations.[20] However, the time and costs involved in analyzing all mutational hot spots in the c-*kit* and *PDGFRA* genes in GISTs present a problem for routine pathologic diagnosis. The results of this study suggest that it is best to analyze mutations in the *PDGFRA* gene first in myxoid epithelioid GISTs with mast cell infiltrations.

In conclusion, we analyzed 30 GISTs that were weak or negative for KIT in this study. We discovered a close correlation between a specific histological type of GISTs, myxoid epithelioid GISTs, and *PDGFRA* gene mutations. Myxoid epithelioid GISTs were accompanied by mast cell infiltrations that were not found in other types of GISTs. These histological characteristics may be useful for subsequent mutational analysis and molecular subclassification of GISTs.

REFERENCES

1. Mazur MT, Clark HB: Gastric stromal tumors: Reappraisal of histogenesis. Am J Surg Pathol 7:507-519, 1983

2. Ueyama T, Guo KJ, Hashimoto H, et al: A clinicopathologic and immunohistochemical study of gastrointestinal stromal tumors. Cancer 69:947-955, 1992

3. Franquemont DW, Frierson HF Jr: Muscle differentiation and

clinicopathological features of gastrointestinal stromal tumors. Am J Surg Pathol 16:947-954, 1992

4. Fletcher CD, Berman JJ, Corless C, et al: Diagnosis of gastrointestinal stromal tumors: A consensus approach. Hum Pathol 33: 459-465, 2002

5. Miettinen M, Lasota J: Gastrointestinal stromal tumors—definition, clinical, histological, immunohistochemical, and molecular genetic features and differential diagnosis. Virchows Arch 438:1-12, 2001

6. Ward SM, Burns AJ, Torihashi S, et al: Mutation of the proto-oncogene c-kit blocks development of interstitial cells and electrical rhythmicity in murine intestine. J Physiol 480:91-97, 1994

7. Burns AJ, Lomax AE, Torihashi S, et al: Interstitial cells of Cajal mediate inhibitory neurotransmission in the stomach. Proc Natl Acad Sci U S A 93:12008-12013, 1996

8. Hirota S, Isozaki K, Yasuhiro M, et al: Gain-of-function mutations of c-kit in human gastrointestinal stromal tumors. Science 279: 577-580, 1998

9. Sarlomo-Rikala M, Kovatich AJ, et al: CD117: A sensitive marker for gastrointestinal stromal tumors that is more specific than CD34. Mod Pathol 11:728-734, 1998

10. Kindblom LG, Remotti HE, Aldenborg F, et al: Gastrointestinal pacemaker cell tumor (GIPACT): Gastrointestinal stromal tumors show phenotypic characteristics of the interstitial cells of Cajal. Am J Pathol 152:1259-1269, 1998

11. Sakurai S, Fukasawa T, Chong JM, et al: Embryonic form of smooth muscle myosin heavy chain (SMemb/MHC-B) in gastrointestinal stromal tumor and interstitial cells of Cajal. Am J Pathol 154: 23-28, 1999

12. Tsujimura T, Makiishi-Shimobayashi C, Lundkvist J, et al: Expression of the intermediate filament nestin in gastrointestinal stromal tumors and interstitial cells of Cajal. Am J Pathol 158:817-823, 2001

13. Rubin BP, Singer S, Tsao C, et al: KIT activation is a ubiquitous feature of gastrointestinal stromal tumors. Cancer Res 61:8118-8121, 2001

14. Heinrich MC, Corless CL, Duensing A, et al: PDGFRA activating mutations in gastrointestinal stromal tumors. Science 299:708-710, 2003

15. Hirota S, Ohashi A, Nishida T, et al: Gain-of-function mutations of platelet-derived growth factor receptor alpha gene in gastrointestinal stromal tumors. Gastroenterology 125:660-667, 2003

16. Wardelmann E, Neidt I, Bierhoff E, et al: c-kit mutations in gastrointestinal stromal tumors occur preferentially in the spindle rather than in the epithelioid cell variant. Mod Pathol 15:125-136, 2002

17. Hasegawa T, Matsuno Y, Shimoda T, et al: Gastrointestinal stromal tumor: Consistent CD117 immunostaining for diagnosis, and prognostic classification based on tumor size and MIB-1 grade. Hum Pathol 33:669-676, 2002

18. van Oosterom AT, Judson I, Verweij J, et al: Safety and efficacy of imatinib (STI571) in metastatic gastrointestinal stromal tumors: A phase I study. Lancet 358:1421-1423, 2001

19. Demetri GD, von Mehren M, Blanke CD, et al: Efficacy and safety of imatinib mesylate in advanced gastrointestinal stromal tumors. N Engl J Med 347:472-480, 2002

20. Heinrich MC, Corless CL, Demetri GD, et al: Kinase mutations and imatinib response in patients with metastatic gastrointestinal stromal tumor. J Clin Oncol 21:4342-4349, 2003

21. Miettinen M, Sarlomo-Rikala M, Lasota J: Gastrointestinal stromal tumors: Recent advances in understanding of their biology. Hum Pathol 30:1213-1220, 1999

22. Maluf HM, Gersell DJ: Uterine leiomyomas with high content of mast cells. Arch Pathol Lab Med 118:712-714, 1994

23. Yavuz E, Gulluoglu MG, Akbas N, et al: The values of intratumoral mast cell count and Ki-67 immunoreactivity index in differential diagnosis of uterine smooth muscle neoplasms. Pathol Int 51:938-941, 2001

24. Ueda T, Aozasa K, Tsujimoto M, et al: Prognostic significance of mast cells in soft tissue sarcoma. Cancer 62:2416-2419, 1988

25. Tomita Y, Aozasa K, Myoui A, et al: Histologic grading in soft-tissue sarcomas. An analysis of 194 cases including AgNOR count and mast-cell count. Int J Cancer 54:194-199, 1993

26. Debiec-Rychter M, Wasag B, Stul M, et al: Gastrointestinal stromal tumors (GISTs) negative for KIT (CD 117 antigen) immunoreactivity. J Pathol 202:430-438, 2004

27. Ward SM, Ordog T, Bayguinov JR, et al: Development of interstitial cells of Cajal and pacemaking in mice lacking enteric nerves. Gastroenterology 117:584-594, 1999

28. Wu JJ, Rothman TP, Gershon MD: Development of the interstitial cell of Cajal: Origin, Kit dependence and neuronal and nonneuronal sources of Kit ligand. J Neurosci Res 59:384-401, 2000

29. Torihashi S, Horisawa M, Watanabe Y: c-kit immunoreactive interstitial cells in the human gastrointestinal tract. J Auton Nerv Syst 75:38-50, 1999

30. Vanderwinden JM, Rumessen JJ, de Kerchove d'Exaerde A Jr, et al: Kit-negative fibroblast-like cells expressing SK3, a Ca2+-activated K+ channel, in the gut musculature in health and disease. Cell Tissue Res 310:349-358, 2002

31. Fujita A, Takeuchi T, Jun H, Hata F: Localization of Ca2+-activated K+ channel, SK3, in fibroblast-like cells forming gap junctions with smooth muscle cells in the mouse small intestine. J Pharmacol Sci 92:35-42, 2003

Bioelectromagnetics 25:599–606 (2004)

Large Scale In Vitro Experiment System for 2 GHz Exposure

Takahiro Iyama,[1]* Hidetoshi Ebara,[1] Yoshiaki Tarusawa,[1] Shinji Uebayashi,[1] Masaru Sekijima,[2] Toshio Nojima,[3] and Junji Miyakoshi[4]

[1]*Wireless Laboratories, NTT DoCoMo, Inc., Yokosuka, Japan*
[2]*Research Division for Advanced Technology, Kashima Laboratory, Mitsubishi Chemical Safety Institute Ltd., Kashima, Japan*
[3]*Division of Media and Network Technologies, Graduate School of Information Science and Technology, Hokkaido University, Hokkaido, Japan*
[4]*Department of Radiological Technology, School of Health Sciences, Faculty of Medicine, Hirosaki University, Hirosaki, Japan*

A beam formed radiofrequency (RF) exposure-incubator employing a horn antenna, a dielectric lens, and a culture case in an anechoic chamber is developed for large scale in vitro studies. The combination of an open type RF exposure source and a culture case through which RF is transmitted realizes a uniform electric field (±1.5 dB) in a 300 × 300 mm area that accommodates 49 35 mm diameter culture dishes. This large culture dish area enables simultaneous RF exposure of a large number of cells or various cell lines. The RF exposure source operates at 2142.5 MHz corresponding to the middle frequency of the downlink band of the International Mobile Telecommunication 2000 (IMT-2000) cellular system. The dielectric lens, which has a gain of 7 dB, focuses RF energy in the direction of the culture case and provides a uniform electric field. The culture case is sealed and connected to the main unit for environmental control, located outside the anechoic chamber, via ducts. The temperature at the center of the tray, which contains the culture dishes in the culture room, is maintained at 37.0 ± 0.2 °C by air circulation. In addition, the appropriate CO_2 density and humidity supplied to the culture case realizes stable long term culture conditions. Specific absorption rate (SAR) dosimetry is performed using an electric field measurement technique and the Finite Difference Time Domain (FDTD) calculation method. The results indicate that the mean SAR of the culture fluid at the bottom of the 49 (7 × 7 array) culture dishes used in the in vitro experiments is 0.175 W/kg for an antenna input power of 1 W and the standard deviation of the SAR distribution is 59%. When only 25 culture dishes (5 × 5 array) are evaluated, the mean SAR is 0.139 W/kg for the same antenna input power and the standard deviation of the SAR distribution is 47%. The proliferation of the H4 cell line in 72 h in a pair of RF exposure-incubators reveals that the culture conditions are equivalent to those of a common CO_2 incubator. Bioelectromagnetics 25:599–606, 2004. © 2004 Wiley-Liss, Inc.

Key words: radiofrequency; SAR; dosimetry; in vitro; temperature regulation

INTRODUCTION

With the widespread use of mobile radio communication systems, many in vitro studies related to radiofrequency (RF) exposure have been conducted. In general, such studies require experimental systems that provide the RF exposure of the cells as well as the stability of the CO_2 density, humidity conditions, and temperature regulation surrounding the cells.

Several kinds of RF exposure systems have been reported for in vitro studies so far. These systems comprise an RF exposure source and an environmental control unit, and they fall into two categories: closed and open types. In the closed type, the RF exposure source is often placed in a common environmental control unit called a CO_2 incubator. In the open type, the environmental control unit is usually self-contained and the RF exposure source is located separately.

For closed type RF exposure systems, the use of a transverse electromagnetic (TEM) cell [Burkhardt et al., 1996], a rectangular waveguide [Schönborn et al., 2000] and a wire patch cell [Laval et al., 2000]

*Correspondence to: Takahiro Iyama, Wireless Laboratories, NTT DoCoMo, Inc., 3-5, Hikari-no-oka, Yokosuka, Kanagawa, 239-8536, Japan. E-mail: iyama@mlab.yrp.nttdocomo.co.jp

Received for review 11 June 2003; Final revision received 26 March 2004

DOI 10.1002/bem.20038
Published online in Wiley InterScience (www.interscience.wiley.com).

have been reported. These methods treat less than 10 samples and fit into common CO_2 incubators. The radial transmission line (RTL) system [Moros et al., 1999] incorporates a self-contained environmental control function and regulates the temperature of the samples, though CO_2 is not provided. Approximately 20 samples can be placed in one RTL. A rectangular waveguide with slits, from which the electromagnetic field leaks and couples to the cell culture, has also been reported [Taki and Suzuki, 2002]. Among the open type RF exposure systems, a far field 2.45 GHz irradiation system [Harrison et al., 1985] in an anechoic chamber provides a 250 × 250 mm cell treatment area and has a self-contained coolant water circulation system to regulate the temperature of the samples. This system requires a large space because the distance between the RF exposure source (a horn antenna) and the samples is greater than 2 m. A cylindrical waveguide [Gajda et al., 2002] allows 1.9 GHz RF exposure of only one sample at the aperture of the waveguide because the distance between the RF exposure source and the sample is 3.2 mm. This system also regulates the sample temperature using a self-contained coolant water circulation system.

As mentioned above, an open type RF exposure system, where the samples are placed in the far field of an RF exposure source, allows many samples to be exposed simultaneously. To achieve simultaneous RF exposure of a large number of cells while minimizing the size of the RF exposure system, we proposed and developed an open type beam formed RF exposure-incubator in an anechoic chamber. In addition, to realize stable long term culture conditions, a self-contained environmental control unit separated from the RF exposure source supplied air at an appropriate temperature, CO_2 density, and humidity to the culture case. This study presents the design of the RF exposure source and the environmental control unit. Data on the specific absorption rate (SAR) distribution in the samples and on the cell culture including the temperature regulation in the culture rooms are also reported. The frequency of 2142.5 MHz, which corresponds to the middle frequency of the downlink band of the International Mobile Telecommunication 2000 (IMT-2000) cellular system, is used in the design of the RF exposure source and in the SAR evaluation.

MATERIALS AND METHODS

System Design

Two identical RF exposure-incubators, one for RF exposure and the other for sham exposure, are established in separate anechoic chambers. A schematic diagram depicting the electrical design and the air circulation of the system is shown in Figure 1A. The RF signal, which is fed from a signal generator (E4437B, Agilent Technologies, Palo Alto, CA) and amplified by a 20 W amplifier (AR Series 2-3 GHz, Comtech PST Corp., Melville, NY), is fed to either RF exposure source located in the respective anechoic chamber. The selection of RF exposure or sham exposure is actuated by mechanical switching in a dummy box. Both the forward and reflected powers are monitored using a 30 dB bidirectional coupler (440964, Microwave Corporation, Cheshire, CT), two power sensors (8481D, Agilent Technologies), and a dual channel power meter (E4419B, Agilent Technologies). All of the equipment except for the RF exposure-incubators is set outside the anechoic chambers in an area called the machine room. Figure 1B is a photograph of the RF exposure-incubator in the anechoic chamber. Customized software on a PC enables control of the frequency, modulation, power level, and exposure time of the RF signal. The PC also records the monitored forward and reflected powers, and the temperature in the culture cases (as described in the Environmental Control Unit).

RF Exposure Source

As shown in Figures 1A and B, the RF exposure source comprising a horn antenna and a dielectric lens radiates RF upwards. The horn antenna, which has an aperture of 187 × 146 mm, is facing upwards, and the dielectric lens, which has a diameter of 430 mm and a relative permittivity of 2.3, is constructed of high density polyethylene and is placed above the antenna. The RF exposure source operates at 2142.5 MHz. The distance between the aperture of the horn antenna and the center of the dielectric lens is 450 mm. The dielectric lens allows RF energy to be focused in the direction of the main beam of the horn antenna. The exposure table constructed of polyester, on which the culture case is set, is 500 mm above the dielectric lens. The height of the exposure table is 1100 mm. Except for the horn antenna and RF connectors, the RF exposure source is constructed using materials of low relative permittivity (less than 5).

Environmental Control Unit

As shown in Figures 1A and B, the culture case made of acrylic material has a two layer structure, that is, the atmosphere in the culture room and that in the air jacket are separated when the front door of the culture case is closed. The main unit, which is located outside the anechoic chambers, provides identical air through sealed ducts at the appropriate temperature (37 °C), CO_2 density (approximately 5%), and humidity (more

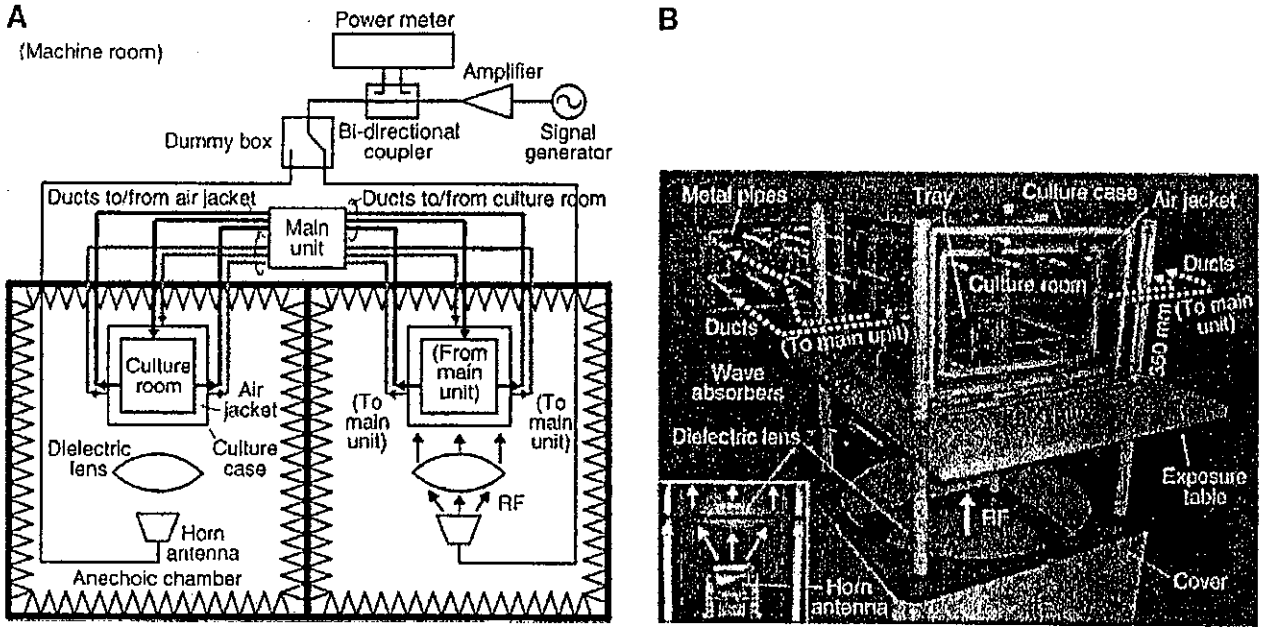

Fig. 1. RF exposure system for in vitro experiments. Arrows from the horn antenna indicate the direction in which the RF travels. **A**: Schematic diagram of the electrical design and the air circulation in the RF exposure system. In this figure, the system on the right is for RF exposure and that on the left is for sham exposure. **B**: Photograph of RF exposure-incubator employing a horn antenna, a dielectric lens and a culture case in an anechoic chamber. Dotted lines indicate the ducts for air circulation. Photograph at the lower left illustrates the inside of the covers of the RF exposure source.

than 90%) for cell culture in the two culture rooms. Warmer air (approximately 40 °C) is circulated in the air jackets through another duct to keep the temperature in the culture room stable. The dimensions of the culture room are $250 \times 400 \times 400$ mm (height × width × depth) and those of the air jacket are $350 \times 500 \times 500$ mm. A tray composed of vinyl chloride plastic is placed at the height of 100 mm from the bottom of the culture room to hold the culture dishes. The tray has a usable area of 340×340 mm corresponding to a 7×7 array of 35 mm diameter Petri dishes. Markings on the tray aid in the placement of the Petri dishes in the same location. The sensing element of a fiberoptic thermometer (AMOTH FL-2000 and FS100-*M, Anritsu Meter Co., Ltd, Tokyo, Japan), which is unaffected by RF, is inserted in the culture room to monitor the temperature. The accuracy of temperature measurement is 0.1 °C.

Anechoic Chamber

To achieve a sufficient degree of isolation between the two culture cases in terms of RF exposure, the RF exposure incubators are placed in separate anechoic chambers. The dimensions of the anechoic chamber are $2.7 \times 2.6 \times 3.95$ m. The ceiling and four side walls including the entrance door are covered with RF absorbers. The shield panels and RF absorbers have an attenuation of greater than 80 dB above 800 MHz and a reflection loss of greater than 40 dB above 2 GHz, respectively. The wall facing the machine room has 12 circular metal pipes, as illustrated in Figure 1B, to which the ducts for air circulation in the culture case (culture room and air jacket) are connected. No RF energy leaks outside the anechoic chamber because the lowest cut-off frequency of the circular metal pipes, which have an inner diameter of 41.6 mm and a length of 220 mm, is 4.2 GHz (for TE_{11} mode). The anechoic chambers are constructed in a clean room (class 10 000) and the temperature is maintained at 22.5 ± 0.5 °C.

SAR Dosimetry

In our studies, adherent cells in a culture fluid with a height of 3 mm are cultivated in 35 mm diameter Petri dishes (353001 FALCON™, Becton, Dickinson and Company, Franklin Lakes, NJ). Therefore, the RF exposure level of the cells is determined as the SAR of the culture fluid at the bottom of the dish. The combination of an electric field measurement technique and the Finite Difference Time Domain (FDTD) [Taflove and Brodwin, 1975a] calculation method was used to assess the SAR distribution in the culture fluid. At 2142.5 MHz, the measurement results using the coaxial probe

(85070C, Agilent Technologies) and the vector network analyzer (8722ES, Agilent Technologies) indicated that the culture fluid had a relative permittivity of 76.4 and a conductivity of 2.5 S/m. The Petri dishes had a relative permittivity of 2.3.

The electric field distribution at the height that the Petri dishes were placed without a culture case was measured using an isotropic electric field probe constructed with three orthogonal 4 mm dipoles (ER3DV6, Schmid & Partners Engineering AG, Zürich, Switzerland) [Schmid et al., 1996], which was calibrated in air. This probe scanned in a 10 mm grid using a robot for industrial use (RX-90, Stäubli AG, Horgen, Switzerland).

It was impossible to measure the SAR in the 3 mm high culture fluid because of the size of the electric field probe. Therefore, the FDTD calculation method was used to evaluate the SAR of the culture fluid at the bottom of the Petri dishes used in the in vitro experiments. To confirm the effectiveness of the FDTD calculation, the SAR distribution in the culture fluid for a large culture dish (135 mm diameter and the fluid height of 18 mm) was measured in 1 mm steps in depth and on a 5 mm grid in the horizontal plane using the same electric field probe, which was calibrated in a liquid having similar permittivity and conductivity to those of the culture fluid used in our in vitro experiments, and scanning facility as described above. The data were compared to the calculated results using the FDTD calculation method assuming that the plane wave was incident from below and the amplitude was the same as the average electric field obtained by the measurement. The voxel size in the vertical direction was 0.5 mm, and that in the horizontal direction was 1.5 mm. The absorbing boundary condition of Mur's second approximation was assumed.

After the effectiveness of the FDTD calculation method was validated, the same calculation algorithm also gave the mean SAR and the SAR distribution in the culture fluid at the bottom of the 49 35 mm diameter Petri dishes used in the in vitro experiments filled with 3 mm high culture fluid. The effect of the culture case was considered negligible because it was constructed from low permittivity materials.

Cell Culture

The temperatures in the two culture rooms were measured using fiberoptic thermometers. The sensing elements of the thermometers were located at the center of each tray in the culture rooms. It was confirmed that the temperature measured using the fiberoptic thermometer was stable within the range of ±0.1 °C even if it was placed in an E field of 100 V/m.

The proliferation of the H4 cell line in the RF exposure-incubators was compared to that in a common CO_2 incubator (BNA-121D, ESPEC CORP., Osaka, Japan). The H4 line of a 37 year old male's human neuroglioma cells obtained from American Type Culture Collection (ATCC; Rockville, MD) was maintained in Dulbecco's Modified Eagle's Medium (high glucose) containing 10% fetal bovine serum (DMEM; GIBCO BRL, Grand Island, NY). Twenty-five (5 × 5 array) 35 mm diameter Petri dishes filled with 3 mm high culture fluid, which contained 3.33×10^4 cells/ml, were placed in each self-contained culture case and a common CO_2 incubator. (The SAR dosimetry results indicated that SAR uniformity for the inner 25 Petri dishes was better than that for the total 49 Petri dishes when the 49 Petri dishes were simultaneously exposed. Therefore, only 25 Petri dishes containing the cells were evaluated in the cell culture test.) At the start of the cell culture test, almost the same number of cells was seeded in the two RF exposure-incubators and the common CO_2 incubator. Both of the RF exposure-incubators were sham exposed. To determine the number of viable cells, cell counting and/or measurement of the level of adenosine triphosphate (ATP) present were performed after 72 h. Cells were counted using a hemocytometer and the ATP level was measured using a luminescent cell viability assay system (CellTiter-Glo™, Promega Corporation, Madison, WI).

RESULTS AND DISCUSSION

SAR Dosimetry

The deviation of the electric field strength at the height that the Petri dishes were placed was ±1.5 dB at 2142.5 MHz in the exposure area (300 × 300 mm) without the culture case. For comparison, it was ±3 dB when the dielectric lens was removed. In addition, the electric field strength measurement with and without the dielectric lens at the center of the exposure area as mentioned above revealed that the gain of the dielectric lens was 7 dB.

The SAR distribution measured in the culture fluid for a large culture dish (135 mm diameter and the fluid height of 18 mm) as shown in Figure 2A and that obtained using the FDTD calculation method were compared while the culture case was not present. Figure 2B illustrates both of the SAR distributions, which are normalized to that obtained using the FDTD calculation method at the bottom of the culture dish, along the central vertical axis. SAR measurement in the culture fluid lower than 5 mm from the bottom of the culture dish could not be performed because the

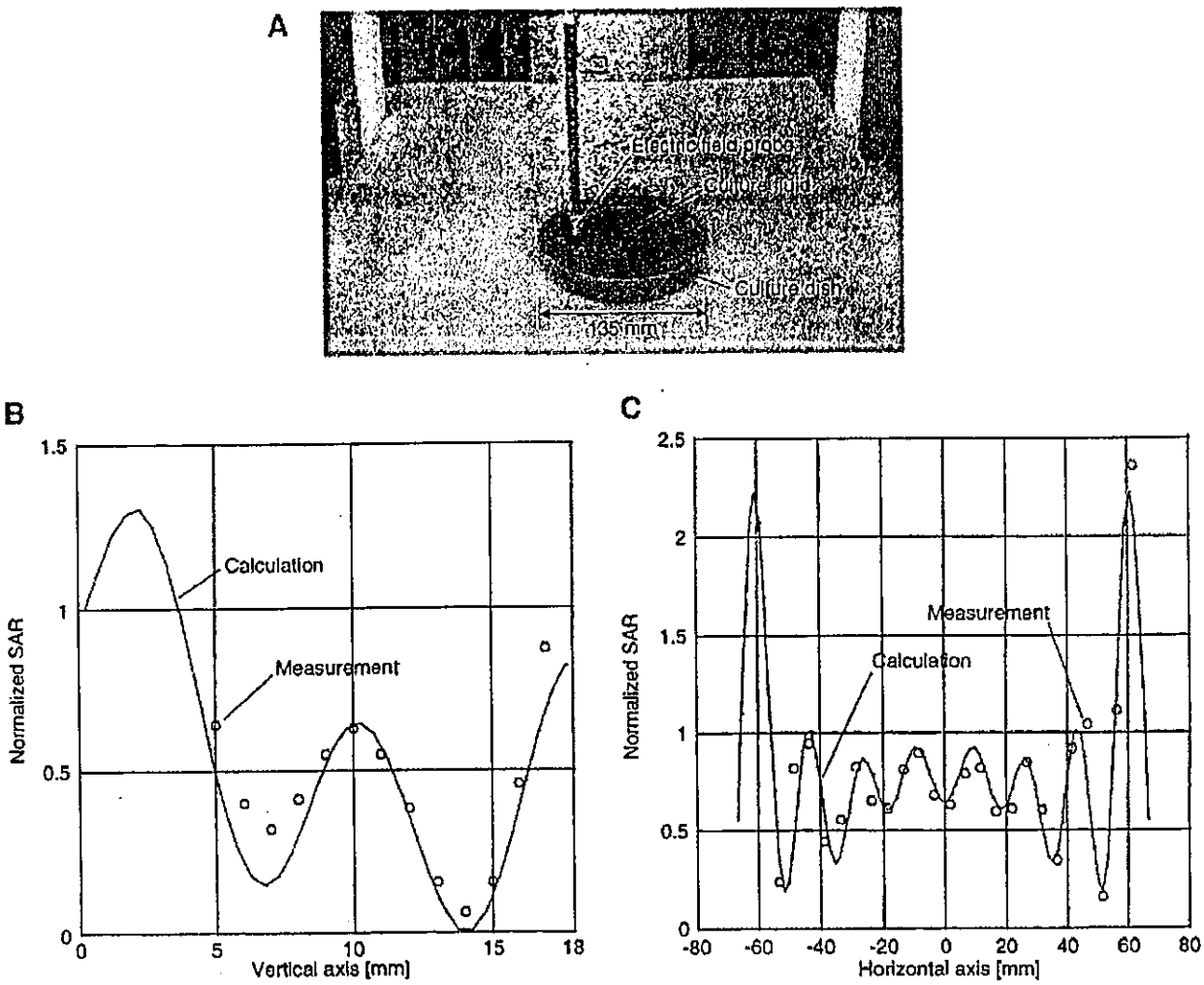

Fig. 2. Comparison of experimental and numerical SAR distributions in the culture fluid in a large (135 mm diameter) culture dish. **A:** Photograph of SAR measurement setup. **B:** The electric field probe scanned along the central vertical axis in 1 mm steps in the culture fluid. **C:** The electric field probe scanned along the horizontal axis 10 mm above the bottom of the dish, along a 5 mm grid in the culture fluid.

distance between the tip and the sensing elements of the electric field probe was approximately 5 mm. The normalized SAR distributions obtained by measurement and calculation along the horizontal axis at the height of 10 mm from the bottom of the dish are shown in Figure 2C. Moreover, two dimensional SAR distributions measured in the culture fluid at the height of 5, 10, and 15 mm from the bottom of the dish on a 5 mm grid revealed that the standard deviations are 19%, 25%, and 60%, respectively. The calculated values were respectively 19%, 31%, and 83%. Although the relatively low SAR level at the height of 15 mm from the bottom of the dish caused some difference in the standard deviation, the measured and calculated results were in good agreement. Totally, the effectiveness of the calculation was confirmed.

The SAR distribution in the culture fluid at the bottom of the 49 35 mm diameter Petri dishes is illustrated in Figure 3A. Moreover, Figure 3B shows the SAR distribution in the culture fluid for the cross section (illustrated as "X-X'" in Figure 3A) of the middle of the tray cutting through seven dishes. Figure 3C illustrates the histogram of the culture fluid at the bottom of the 49 35 mm diameter Petri dishes. Assuming that an incident electric field has the same amplitude as the average electric field in the exposure area for the antenna input

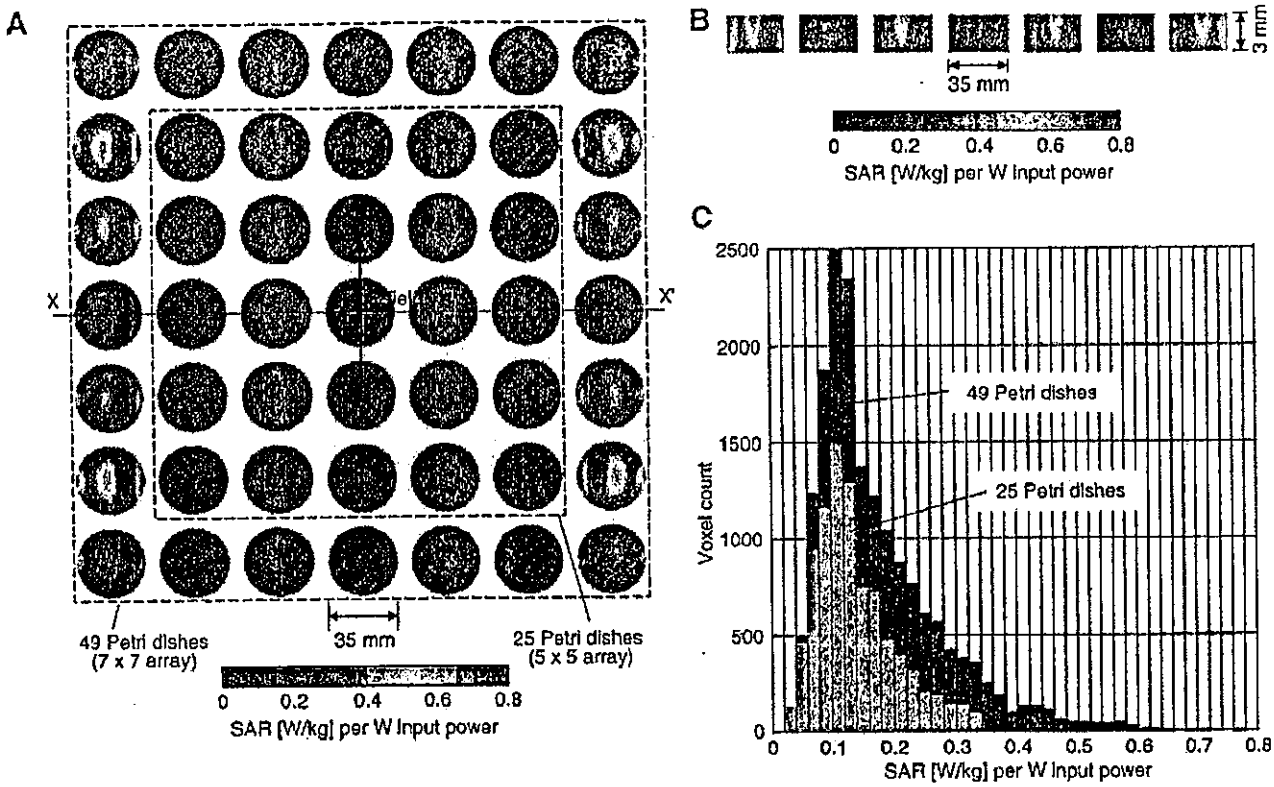

Fig. 3. Calculated SAR distributions in the culture fluid in Petri dishes used in the in vitro experiments (35 mm diameter). **A**: At the bottom of the 49 Petri dishes the electric field is depicted from the bottom up. **B**: A cross section (illustrated as "X-X'" in Fig. 3A) of the middle of the tray cutting through seven Petri dishes. **C**: Histogram at the bottom of the 49 and 25 Petri dishes.

power of 1 W by measurement, the mean SAR was 0.175 W/kg. For example, to achieve a mean SAR of 0.08 W/kg, which corresponds to the basic restriction for general public exposure recommended by International Commission on Non-Ionizing Radiation Protection (ICNIRP) [ICNIRP, 1998], an antenna input power of 0.46 W is required. An antenna input power of 11.4 W leads to a mean SAR of 2.0 W/kg. The standard deviation of the SAR distribution was 59%. When the SAR distribution in the culture fluid at the bottom of the inner 25 Petri dishes (5 × 5 array) was evaluated as illustrated in Figure 3C, the mean SAR was 0.138 W/kg for an antenna input power of 1 W and the standard deviation of the SAR distribution was 47%. Here, the remaining 24 of the 49 Petri dishes were assumed to be exposed simultaneously.

Schönborn et al. [2001] summarized the standard deviations of the SAR distribution in the culture fluid at the bottom of 60 mm diameter Petri dishes in closed type RF exposure systems. TEM cells provide a standard deviation of approximately 15% at 835 MHz when only two dishes are used. At 1.62 GHz, a standard deviation of approximately 30% is achieved using an RTL and a rectangular waveguide. The standard deviations of the SAR distribution in open type RF exposure systems have not been previously reported in detail. However, Guy et al. [1999] reported that plane wave exposure resulted in a standard deviation of more than 100% at the bottom of four T-25 flasks at 2450 MHz. Our system provides an equivalent uniformity of SAR distribution compared to other systems. Large-scale cell culture corresponding to the placement of 49 35 mm diameter Petri dishes with reasonable SAR uniformity contributes to large scale in vitro experiments.

If the RF exposure level is relatively high, significant heat due to RF exposure in the culture fluid may be expected. Although air at 37 °C flows constantly in the culture room and excludes the heat in the culture fluid caused by RF exposure to a certain extent, we expect that we need to increase the capabilities of our system to exclude a significant rise in temperature due

to high level RF exposure in the culture fluid. When the mean SAR is 0.08 W/kg, we confirmed that the rise in the temperature in the culture fluid is less than 0.1 °C by the measurement using the fiberoptic thermometers and the calculation based on the heat conduction equation [Taflove and Brodwin, 1975b]. Therefore, for lower level RF exposure such as that by mobile radio base stations, there is no need to consider the temperature change in the culture fluid.

Cell Culture

The temperature change over 72 h in each culture room was less than 0.2 °C, whereas that in the machine room was more than 2.0 °C, as shown in Figure 4A. It was also confirmed that the temperature recovery in the culture room required 18 min to reach 36.5 °C and at most 72 min to reach 37.0 °C after opening the front door of the culture case for 30 s. Figure 4B shows the number of H4 cells in the incubators after 72 h. The cell count was 62 ± 8.1, 62 ± 4.6, and 60 ± 9.2 (mean $\pm$ standard deviation) $\times 10^4$/dish in RF exposure-incubators 1 and 2 (both sham exposed) and the common CO_2 incubator, respectively. No statistically significant difference was exhibited among them. A comparison of ATP levels after 72 h is illustrated in Figure 4C. The ATP levels were 8409 ± 2480, 8717 ± 1712, and 9065 ± 3021 nmol/dish in RF exposure-incubators 1 and 2, and the common CO_2 incubator, respectively. These results also showed no statistically significant difference among them. It was confirmed that the culture conditions of our RF exposure-incubators were equivalent to those of a common CO_2 incubator. Maintenance of the appropriate temperature, CO_2 density, and humidity realized stable long term culture conditions.

CONCLUSION

A beam formed RF exposure-incubator for in vitro experiments has been presented. Its important features are that the combination of an open type RF exposure source and a self-contained environmental control unit established large scale and long term cell culture conditions, and that a dielectric lens focused RF energy in the direction of the culture case and provided a uniform electric field as well as minimizing the size of the RF exposure system.

Since the electric fields are parallel to the culture fluid layer, the standard deviation of the SAR distribution in our system is slightly larger than those in systems where the electric fields are normal to the culture fluid layer. For example, our system achieves standard deviations of 59% and 47% for 49 and 25 culture dishes, respectively. The efficiency in our system, which is

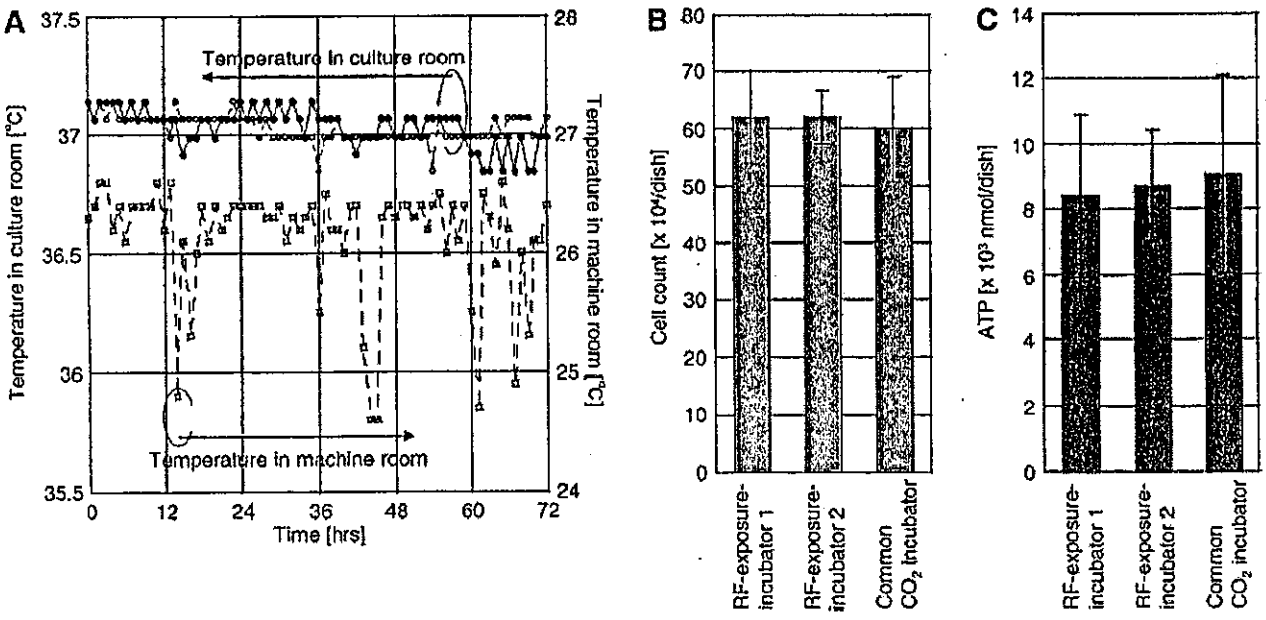

Fig. 4. Culture conditions in the RF exposure-incubators. **A**: Temperature regulation in two culture rooms over 72 h. **B**: Counts of the H4 cell lines in the two RF exposure-incubators and in the common CO_2 incubator after 72 h. **C**: ATP levels of the H4 cell line in the two RF exposure-incubators and in the common CO_2 incubator after 72 h.

equivalent to an RTL, provides a sufficient SAR level in our in vitro experiments with an acceptable standard deviation of the SAR distribution.

If the RF exposure level is at such a high level that it causes a significant rise in the temperature in the culture fluid, we expect that we need to increase the capabilities of our system to exclude a significant rise in temperature due to high level RF exposure. However, we have confirmed that a mean SAR of 0.08 W/kg at the bottom of the culture fluid, which corresponds to the basic restriction for general public exposure recommended by ICNIRP, causes a temperature rise of less than 0.1 °C. Therefore, our system can effectively simulate RF exposure from mobile radio base stations without the need to consider the heat in the culture fluid. In addition, to achieve a mean SAR of 0.08 W/kg at the bottom of the 49 or 25 culture dishes, input powers of 0.46 W or 0.59 W are required, respectively. This indicates that conventional amplifiers can be used to simulate such RF exposure of cells.

Large scale cell culture enables RF exposure of various cell lines and allows us to obtain highly accurate and reliable in vitro statistical data through the analysis of an extremely large number of cells. Observation of continual changes in the cells can also be realized. Using an RF exposure system, we will conduct in vitro experiments for low level, long term exposure by 2 GHz radiation, including gene analysis.

REFERENCES

Burkhardt M, Poković K, Gnos M, Schmid T, Kuster N. 1996. Numerical and experimental dosimetry of Petri dish exposure setups. Bioelectromagnetics 17:483–493.

Gajda GB, McNamee JP, Thansandote A, Boonpanyarak S, Lemay E, Bellier PV. 2002. Cylindrical waveguide applicator for in vitro exposure of cell culture samples to 1.9-GHz radiofrequency fields. Bioelectromagnetics 23:592–598.

Guy AW, Chou CK, McDougall JA. 1999. A quarter century of in vitro research: A new look at exposure methods. Bioelectromagnetics 20(Suppl 4):21–39.

Harrison GH, McCulloch D, Balcer-Kubiczek EK, Robinson JE. 1985. Far-field 2.45 GHz irradiation system for cellular monolayers in vitro. J Microw Power 20:145–151.

International Commission on Non-Ionizing Radiation Protection (ICNIRP). 1998. Guidelines for limiting exposure to time varying electric, magnetic and electromagnetic fields (up to 300 GHz). Health Phys 74:494–522.

Laval L, Leveque PH, Jecko B. 2000. A new in vitro exposure device for the mobile frequency of 900 MHz. Bioelectromagnetics 21:255–263.

Moros EG, Straube WL, Pickard WF. 1999. The radial transmission line as a broad-band shielded exposure system for microwave irradiation of large numbers of culture flasks. Bioelectromagnetics 20:65–80.

Schmid T, Egger O, Kuster N. 1996. Automated E-field scanning system for dosimetric assessments. IEEE Trans Microw Theory Tech MTT 44:105–113.

Schönborn F, Poković K, Wobus AM, Kuster N. 2000. Design, optimization, realization, and analysis of an in vitro system for the exposure of embryonic stem cells at 1.71 GHz. Bioelectromagnetics 21:372–384.

Schönborn F, Poković K, Burkhardt M, Kuster N. 2001. Basis for optimization of in vitro exposure apparatus for health hazard evaluations of mobile communications. Bioelectromagnetics 22:547–559.

Taflove A, Brodwin ME. 1975a. Numerical solution of steady-state electromagnetic scattering problems using the time-dependent Maxwell's equations. IEEE Trans Microw Theory Tech MTT 23:623–630.

Taflove A, Brodwin ME. 1975b. Computation of the electromagnetic fields and induced temperatures within a model of the microwave-irradiated human eye. IEEE Trans Microw Theory Tech MTT 23:888–896.

Taki M, Suzuki Y. 2002. Dosimetry for in vitro study on non-thermal biological effects of microwaves. Proc Int Symp Bioelectromagnetics 24–27.

The Role of DNA-Microarray in Translational Cancer Research

Sönke Korfee[1], Wilfried Eberhardt[2], Yasuhiro Fujiwara [3] Kazuto Nishio[1]

1 Shien Lab, National Cancer Center Hospital Tsukiji 5-1-1, Chuo-ku, Tokyo 104-0045, JAPAN

2Department of Internal Medicine (Cancer Research) ,West German Cancer Centre, Hufeland Strasse 55,45122 Essen, Germany

3Breast and Medical OncologyDivision, National Cancer Center Hospital Tsukiji 5-1-1, Chuo-ku, Tokyo 104-0045, JAPAN

Abstract:

The overall prognosis for the majority of cancer patients remains poor. Current conventional strategies in clinical cancer research are not able to adequately answer a large number of important questions. Although some patients achieve substantial benefits from classical cytotoxic chemotherapy others, will not. The mechanisms behind this phenomenon are still not in detail identified. Furthermore, the activity of promising novel molecular targeting anticancer agents like tyrosine kinase inhibitors is currently not predictable in the individual patient. The biological background for this clinical and prognostic heterogeneity in behaviour is more or less the large individual variation in the biological nature of tumors within the same classified histological subgroup.The usefulness of conventional histological classifications to predict patient prognosis or response to chemotherapy is definitely limited. The most promising way to improve this situation is to build clinical research strategies on intricate biological evidence. New genomic technologies have been developed within the recent years. These techniques are able to analyze thousands of genes and their expression profiles simultaneously. An increasing number of investigations has been reported looking at the application of these novel technologies within the setting of clinical trials. The purpose of this approach is to discover new subsets of cancer patients, to improve prediction of the clinical outcome of disease or response to treatment and select new targets for novel agents with innovative mechanisms of action based on the findings from gene expression profiles. Results of these gene expression profiling based studies could potentially lead to more individually tailored systemic cancer therapy. In the recent years a remarkable number of studies based on these techniques has already been reported. Although the published results are in general impressive and highly promising, a lot of work still remains to be done. Moreover, there is a strong need for an increase in reliability and reproducibility of gene expression profiling techniques and thus introduction of quality assurance in the performance of these assays. Although a large number of issues remain to be clarified prior to a more general application of genomic profiling techniques in clinical cancer research, this strategy will eventually turn out as a promising approach to improve successful management of cancer patients.

Introduction:

The overall prognosis for the majority of cancer patients is still rather unsatisfactory.Hardly any stage IV lung cancer patient is alive five years following following initial diagnosis [Mountain 1997].Even new generation cytotoxic agents with higher efficacy and more favourable toxicity profiles such as paclitaxel, docetaxel and gemcitabine have not brought an identifiable breakthrough in cancer therapy [Schiller 2002]. A large group of tumor entities is primarily resistant or will develop secondary resistance to cytotoxic chemotherapy. On the other hand, there is a definite subset of patients with an identifiable benefit from cancer chemotherapy. The basic mechanisms behind this clinical phenomenon remain not clearly identified. Adjuvant chemotherapy following definitive local treatment (e.g complete resection) of early disease is another important issue. In earlier stages with the opportunity for intended curative surgical treatment, there is currently no reliable method to predict which patient will have a significant benefit from adjuvant treatment.The current situation regarding the use of novel molecular targeting drugs is of striking parallelity. Activity of these agents is at the moment not at all be predictable in individual patient. A substantial reason for this situation in current clinical cancer research are the remarkable individual varities in the biological nature and clinical behaviour of tumors even within the same pathological entity. The usefulness of classical histological subclassifications to predict patient prognosis or response to chemotherapy is definitely limited. Introducing more information on tumor biology from basic research results to clinical investigations is supposed to improve cancer treatment strategies in the future. This approach could be one important step to individualize cancer management. New genomic technologies have been developed within the recent years. These techniques have the capability to analyze the expression and activity of thousands of different genes simultaneously. An increasing number of investigations has applied these genomic techniques as an adjunct to their clinical studies with the

purpose to discover new (sub)-classes of tumors or predict outcome of therapy on the basis of these gene expression profiles. Although a number of studies has been published during the last years with impressive and clinical relevant results, a lot of work remains to be done. One major challenge will be to find the appropriate statistical method for analyzing the large data sets correctly to get valid and reliable scientific results. Currently, another major problem is the lack of comparability between results from different investigations. Several different genomic techniques (cDNA-microarray, filter-array, short and long oligonucleotide arrays), statistical methods (supervised and unsupervised analysis) have been used in recent clinical investigations. International standardizations of gene profiling based studies is needed for a proper interpretation of results in the future. In spite of a large number of unsolved issues when applying genomic techniques to clinical cancer research, these methods still belong to the most promising tools to improve treatment results within the future. The current role of genomic techniques in translational cancer research will be analyzed in the following overview. In the first part of this paper we will summarize the most important studies for frequent cancer entities published. Furthermore, the applied methods and their clinical relevance will be critical reviewed. In the second part of the manuscript, we will focus on the reliability and the reproducibility of reported genomic array data.

Breast Cancer

In 2000 a Norwegian – American Cooperative Group performed an analysis of breast cancer cell lines and tumor tissue based on DNA microarrays [Perou 2000]. They could classify the tumors into subtypes distinguished by their different gene expression profiles using the "hierarchical clustering [1]" methology based on 1753 genes independent from the histological classification The tumors were subdivided into an ER+(estrogen-receptor-positive)/luminal like, a basal-epithelium-